Regular Article

PHYSICAL CHEMISTRY RESEARCH
Published by the
Iranian Chemical Society
www.physchemres.org
info@physchemres.org

Phys. Chem. Res., Vol. 11, No. 4, 707-723, December 2023
DOI: 10.22036/pcr.2022.353920.2192

Towards Screening and Repurposing of Approved Drugs for the Treatment of COVID-19 Using Molecular Docking

M. Soltani[a], S. Sardari[b], H. Sabzyan[c,*] and F. Ghasemi[a,d,*]

[a]*Department of Bioinformatics and Systems Biology, School of Advanced Technologies in Medicine, Isfahan University of Medical Sciences, Isfahan, 81746-73461, I. R. Iran*

[b]*Drug Design and Bioinformatics Unit, Department of Medical Biotechnology, Biotechnology Research Center, Pasteur Institute of Iran, Tehran 13169-43551, I. R. Iran*

[c]*Department of Chemistry, University of Isfahan, Isfahan 81746-73441, I. R. Iran*

[d]*Bioinformatics Research Center, School of Pharmacology and Pharmaceutical Sciences, Isfahan University of Medical Sciences, Isfahan, 81746-73461, I. R. Iran*

(Received 11 September 2022, Accepted 2 November 2022)

Molecular docking was applied to investigate interactions between 1638 approved drugs, SARS-CoV-2 virus proteins (spike, non-structural proteins NSP3, NSP7, NSP8, NSP9, NSP10, NSP12, NSP15, NSP16, and NSP10-NSP16 complex), and the human angiotensin-converting enzyme 2 (ACE2) protein and its Spike@ACE2 complex. Structures of these approved drugs were fully optimized using the universal force field (UFF), and their lowest energy conformations were used for docking on the (co)crystallized structures of the target proteins taken from the protein data bank (PDB). The docking procedure was performed in two stages, and the results were evaluated based on four docking scores (ranking indices), which were used to measure the comparative affinities of the studied drugs towards the SARS-CoV-2 virus proteins. Details of the positions, orientations, and interactions of the first three highest-ranked drugs in the binding pocket of the COVID-19 spike, NSP7, and human ACE2 proteins (as representatives) were visualized and analyzed. Based on the results of this molecular docking study, vazegepant, dasabuvir, vitamin E, fosamprenavir, raltegravir, canagliflozin, biliverdin, and imatinib drugs can be considered promising for further molecular mechanics/dynamics simulations and clinical studies to improve the screening process.

Keywords: COVID-19, Spike and NSP proteins, Repurposing, Molecular docking, ACE2, Ranking indices

INTRODUCTION

COVID-19 is an acronym standing for corona (CO) virus (VI) disease (D) that emerged in 2019 (19). In the early stage of the epidemic, the strongly contagious SARS-CoV-2 virus was known as the 2019 novel coronavirus abbreviated as 2019-nCoV. Further studies showed that this virus was linked to the virus family of the severe acute respiratory syndrome (SARS) and thus was named SARS-CoV-2. This virus is similar to some types of common cold viruses [1]. The novel transmissible infectious disease COVID-19 emerged as a global disaster due to the absence of vaccination or any definite drugs that could be used for effective treatment. Since its emergence, COVID-19 has spread worldwide very quickly and become a pandemic by infecting about 633 million people (7/11/2022), out of which more than 6.5 million have lost their lives. These data can be compared with what was reported for SARS (774 deaths in 2003) and MERS (866 deaths during 2012-2020) [2]. Intensive efforts by health researchers in many countries have so far resulted in the preparation, successful tests, registration, and application of several vaccines, including Pfizer-BioNTech, Moderna, AstraZeneca, Sputnik V, Sinovac, Sinopharm, Covaxin,

*Corresponding authors. E-mail: sabzyan@sci.ui.ac.ir; f_ghasemi@amt.mui.ac.ir

Novavax, Janssen/Johnson&Johnson, and Baharat Biotech. In addition, a number of other vaccines, such as COVIran Barakat, Cuba-Iran Soberana, Fakhra, and Razi-Cov-Pars have been approved and are being used locally. To date, more than 12.4 billion doses of these vaccines have been successfully administered [1].

Accurate knowledge of SARS-CoV-2 virus genome components, including its structural and functional proteins and their response to any proposed drugs, is necessary for the development of any successful treatment protocol. The single-strand RNA of the coronavirus genome contains ~30000 nucleotides and consists of two large genes. One of these genes encodes four structural proteins, namely, spike (S), membrane (M), nucleocapsid, (N), and envelope (E) proteins, and the other encodes 16 non-structural proteins (NSP1-NSP16). The viral surface proteins S, E, and M are embedded in the lipid bilayer. The membrane protein (M) plays a central role in organizing coronavirus structure since its abundance is the highest among the viral surface proteins. The envelope protein E is a small membrane protein composed of 76-109 amino acids and minor components of the virus particle. A model structure of the COVID-19 virus surface is shown in Fig. 1. The set of 16 non-structural proteins (NSPs) are arranged inside the virus and are not shown in Fig. 1.

The spike (S) glycoprotein is known to mediate the attachment of the SARS-CoV-2 virus to the human host cell-surface receptor (angiotensin-converting enzyme 2, ACE2). This attachment is a primary step towards the fusion of the membranes of the SARS-CoV-2 virus and human cell, which eventually leads to the entry of the virus into the human host cell. The spike glycoprotein contains 1273 amino acids and consists of two S1 and S2 protein domains (subunits), which function in the recognition and fusion processes, respectively [3]. The COVID-19 virus (SARS-CoV-2) has two proteases, named the papain-like protease (PL^{pro}) and the chymotrypsin-fold main protease (M^{pro} or $3CL^{pro}$). In the vital proteolytic process, M^{pro} ($3CL^{pro}$) protease releases the functional proteins spike, membrane, envelope, nucleoprotein, replicas, and polymerase from the virus polyproteins [3]. The PL^{pro} enzyme manages the processing of the viral polyproteins for the generation of the functional replicase complex, which is an essential step in the spread of the virus [4].

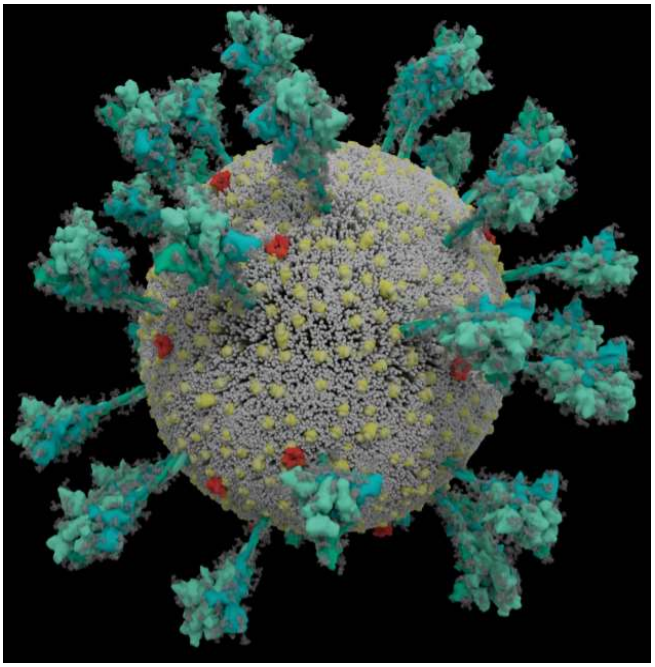

Fig. 1. A model structure of the Covid-19 virus surface. The surface proteins spike (S), membrane (M), and envelope (E) are highlighted in blue, yellow, and red, respectively. This model was taken with permission from Dr. Janet Iwasa of the Department of Biochemistry, University of Utah (color online).

To date, a number of drug groups, including (i) favipiravir, amantadine, baloxavir marboxil, oseltamivir, umifenovir, zanamivir, and molnupiravir, (ii) PF-00835231 and ribavirin, (iii) remdesivir and galidesivir, and (iv) indinavir, ivermectin, tipranavir, and Tenofovir (v), have been examined, prescribed, and used as part of the COVID-19 treatment based on their relative success in the treatment of some relevant viruses, including influenza, SARS-COV-1, Ebola, and HIV, respectively [5]. Recent clinical reports have shown that none of these drugs provided satisfactory results to be nominated as specific and definite drugs for curing or controlling the propagation of COVID-19 [6-7]. It is worth noting that the antiviral molnupiravir has been reported to be effective and safe in reducing the risk of severe engagement and mortality in high-risk groups infected with mild to moderate COVID-19.

Achieving the most appropriate and effective COVID-19 treatment *via* routine experimental methods is very expensive

and time-consuming and sometimes requires several years of research to reach the stage of clinical approval [8]. Furthermore, experimental methods of drug discovery and development are always associated with a certain risk of infection for researchers. Obtaining a complete molecular picture of the drug-target interactions requires physical presence in the laboratory and delivery of the viral species in different experiments, which increases the risk of contamination. An alternative method to effectively screen appropriate drugs for treating COVID-19 is to apply computational techniques to design and engineer new drugs and investigate the feasibility of the application of already approved drugs. This latter approach, also known as *drug repurposing* or *drug repositioning*, is a cost-effective method to battle any new rapidly spreading diseases, specifically those caused by viruses. The much shorter time required in computational techniques compared to that in experimental approaches is an advantage for screening approved and available drugs to evaluate their potential applications for the treatment of COVID-19. Moreover, computational techniques allow researchers to predict the adverse effects and potential risks associated with candidate drugs. The results of such computational studies, however, need clinical trials for overall evaluations and final approval.

Molecular docking is one of the commonly used structure-based methods for the evaluation of drug-protein binding (Gibbs free energies). For this purpose, the energies of non-covalent protein-ligand interactions, including van der Waals and coulomb and hydrogen bond interactions, are calculated. In these calculations, various positions, orientations, and conformations of the proposed drug molecule in the binding site(s) of the receptor macromolecule (protein) are considered. The most probable positions, orientations, and conformations are then scored based on the calculated affinities.

A large number of molecular docking and molecular dynamics (MD) simulation studies have been carried out so far to identify prospective effective drugs inhibiting the SARS-CoV-2 virus. In an early study, a molecular docking method was used for the virtual screening of some novel clinically approved drugs considered to play the role of coronavirus protease inhibitors [9]. In this docking study, the structure of COVID-19 M^{pro} ($3CL^{pro}$) extracted from XRD data was used and the relative affinities of the drugs towards COVID-19 M^{pro} ($3CL^{pro}$) were evaluated. Among the drugs considered in the screening, saquinavir and beclabuvir were identified as the most effective candidates for the treatment of COVID-19. In another recent study, molecular docking was used to identify disulfiram (DSF) derivatives as probable inhibitors against SARS-CoV-2 (PL^{pro}) [10]. In the period between the two above-mentioned studies, many studies have been carried out employing computational molecular docking approaches to find effective inhibitors of SARS-CoV-2 proteins M^{pro} ($3CL^{pro}$), PL^{pro}, spike (S), and a few non-structural proteins. These studies, which have focused on different approved drugs and their derivatives, have led to the identification of potential inhibitors against COVID-19 disease [11-48]. A summary of some of these studies is given in Table S1 (Supplementary Materials). In addition, some studies have employed MD simulation to investigate the intermolecular stability and dynamics of the complexes between the COVID-19 proteins and some drugs proposed as their inhibitors [11-25]. For example, in one study, the interactions between drug-like compounds and existing approved drugs with M^{pro} ($3CL^{pro}$) were investigated using high-throughput molecular docking. In addition, MD simulations were carried out on five selected compounds to validate their stabilities and interactions with M^{pro} ($3CL^{pro}$) [11]. To our knowledge, no comprehensive study has reported on the molecular docking study of the interactions between the approved drugs and all important proteins of COVID-19 at the same time. Different researchers have used different sets of COVID-19 proteins in their studies.

In the present study, the interactions between the approved drugs and the COVID-19 proteins, including spike (S), non-structural proteins NSP3, NSP7, NSP8, NSP9, NSP10, NSP12 (two sites), NSP15, NSP16, and a protein pair complex (NSP10-NSP16), were investigated using molecular docking. In addition, the interactions between the approved drugs and the human host cell ACE2, as the directly attacked protein by the guest COVID-19 spike protein, and its complex with the spike protein (*i.e.*, Spike@ACE2) were examined. The drugs used in the present study were ranked based on four ranking indices calculated based on their interaction free energies. Details of these docking studies and their results are described and discussed below.

MATERIALS AND METHODS (COMPUTATIONAL DETAILS)

Ligands Preparation

Two-dimensional molecular structures of a total number of 2200 compounds, registered as investigated and approved drugs, were taken in SDF format from the PubChem and DrugBank databases. These drugs included, but were not limited to, antitumor, anti-diabetic, antimalarial, and antiviral agents. In a preliminary screening stage, the approved drugs with polypeptide structures, those with molecular weights above 700 g mol^{-1}, and those prescribed for cancer and nervous disorders were removed from the initial list of compounds. To evaluate and rank the efficiencies of the remaining 1638 compounds for the treatment of COVID-19 disease, their molecular structures were studied using GaussView software [49]. After initial refining (in cases required), their three-dimensional structures were built, modeled, and optimized using a molecular mechanics method with the UFF [50], as implemented in Gaussian 09 [51]. The UFF-optimized structures were then converted to the PDB file format using GaussView software to be later used to prepare the structures of docking complexes.

Target Selection and Preparation

The crystal structures of COVID-19 proteins were taken from the PDB database in PDB format [52]. These proteins included closed state spike glycoprotein (6VXX), spike receptor binding domain bound to ACE2, *i.e.* Spike@ACE2 (6M0J), ADP ribose phosphatase NSP3 in the complex with ADP ribose (6W02), NSP15 endoribonuclease (6VWW), NSP9 RNA binding protein (6W4B), the NSP10-NSP16 protein complex (6W4H), and the NSP12-NSP7-NSP8 protein complex as bound to the template-primer RNA and triphosphate form of Remdesivir (7BV2). In the present docking study, individual constituent proteins of the two complexes (*i.e.*, NSP10-NSP16 and NSP12-NSP7-NSP8) were isolated and their interactions with the drugs were studied. Moreover, the structure of the human protein ACE2 was extracted from the Spike@ACE2 complex, and the interactions between the drugs with the isolated ACE2, along with its complex, and spike (Spike@ACE2) were studied. The interactions between the drugs with the NSP10-NSP16 complex were also simulated. Therefore, the drug-receptor pairs considered in this molecular docking study included the following: (1) drug-spike, (2) drug-Spike@ACE2, (3) drug-ACE2, (4) drug-NSP3, (5) drug-NSP7, (6) drug-NSP8, (7) drug-NSP9, (8) drug-NSP10, (9) drug-NSP12, (10) drug-NSP12(R), (11) drug-NSP15, and (12) drug-NSP16, and (13) drug-(NSP10-NSP16). In all docking studies on the spike glycoprotein (6VXX), only the A (alpha) chain of its three identical (A, B & C) chains was considered.

In the first step, water molecules and accompanying species (*i.e.*, cations, anions, and/or ligands) were removed from the initial crystal structures of all proteins by either using Autodock4 software or removing the lines of the corresponding atoms during the preparation of the PDB input files. The missing hydrogen atoms and the Gasteiger atomic charges were also added to the PDB files. The PDB files of the receptor targets (proteins) were converted to appropriate file formats (PDBQT), readable by the AutoDock4/AutoDock Vina software, as input of the molecular docking [53-54]. Openbable software was used to convert the PDB files of the drugs to their corresponding PDBQT formats [55]. The ligand-protein (drug-protein) complex in the simulation box was prepared in the AutoDock software by merging the individual PDBQT files of the ligands (drugs) and the protein.

Examples of the setting of the grid search boxes at the active sites (binding pockets) of the receptor proteins used in this docking study are shown in Fig. 2. In some cases, more than one box was used to ensure that all possible interaction sites and configurations were included in the docking procedure. As an example, for NSP12, two boxes were selected, of which one covered the NSP8-NSP12 junction and the other covered the Remdesivir binding site (Fig. 2), as reported in Ref. [56]. Dimensions of the search grid box in the x, y, and z directions were set in the range of 40-126 Å depending on the protein (receptor). Also, a uniform grid spacing of 0.375 Å was considered for all dockings. The center of the grid box was set appropriately to allow all possible interactions at different positions, orientations, and conformations of the drug molecule and to assure the required binding flexibilities at the docking site. The interaction grid maps were generated using the AutoGrid module of AutoDock.

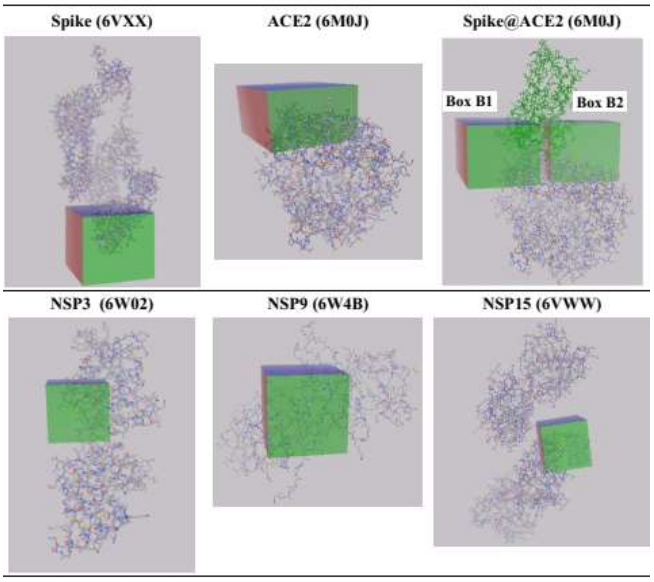

Fig. 2a. The docking search boxes set at the interaction active sites of the receptor proteins spike (6VXX), ACE2 (from 6M0J), ACE2@Spike (6M0J), NSP3 (6W02), NSP9 (6W4B), and NSP15 (6VWW). Note that the sizes of different parts are not to scale (color online).

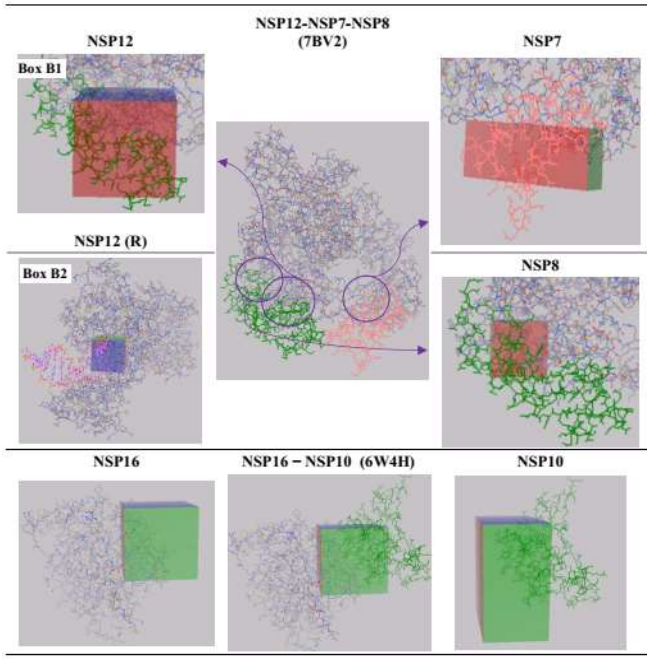

Fig. 2b. The same as Fig. 2a, but the structures of NSP7, NSP8, and NSP12 proteins were extracted from the structures of NSP12-NSP7-NSP8 complex (7BV2) and NSP16-NSP10 (6W4H) complex and its components NSP10 and NSP16 proteins. Note that the sizes of different parts are not to scale (color online).

Molecular Docking

Docking details. The ligand-receptor binding modes and the key interactions between the highest-ranked compounds and target proteins were determined based on the results obtained from docking analyses using the AutoDock program (version 4.2.6). In these analyses, free energy function and Lamarckian genetic algorithm with local research were used. The receptor was set as a rigid body whereas the ligands were allowed to be flexible so that all possible conformations with respect to the receptor active site atoms could be adopted.

The lowest energy conformations of the 1638 drugs considered in this study were docked on the COVID-19 spike, NSP, and the human ACE2 proteins using 10 independent docking runs. The Gibbs free energies of the drug-protein interactions obtained in this docking screening stage were used to calculate the ranking index r_b (Eq. (2)). Then, a set of 213 drugs was prepared from the collection (union) of the first 50 drugs having the highest r_b scores (ranking index) for each COVID-19 protein. A more accurate docking procedure, with 150 independent docking runs, was carried out on the interactions between these screened drugs and the COVID-19 spike, NSPs, and the human ACE2 proteins. Other parameters of the search algorithm of the docking procedure were set at their default (program) values. The interaction Gibbs free energies obtained at this stage were used to calculate the four ranking indices (docking scores) r_a, r_b, r_c, and r_d, introduced in Eqs. ((1)-(4)) in Section 2.3.2.

It is known that the COVID-19 spike protein initiates the viral infection process by its interaction with the ACE2 protein of the host human cells [57]. Therefore, the ACE2 protein is the most relevant and representative human receptor that can be considered as the reference (control) protein to evaluate the side effects of the examined drugs. That is, the drugs having respectively the strongest and weakest interactions with COVID-19 proteins and the human ACE2 protein may be more effective in inhibiting the SARS-CoV-2 virus and thus should be scored higher and screened for the next stage in the drug design procedure. To consider other human proteins as the reference, detailed molecular structures of their ligand-receptor complexes are required that are not presently available. Therefore, ACE2 protein is the only representative human protein that can be considered as a reference for the present study. The three ranking indices

(docking scores) r_b, r_c , and r_d (Eqs. (2)-(4)) were defined, calculated, and analyzed for this purpose.

Ranking indices (docking scores). Evaluation of the relative efficiencies of the studied drugs in inhibiting the COVID-19 virus proteins was based on a number of ranking indices defined in terms of the Gibbs free energies of the interaction, which measure comparative drug-receptor binding strengths, between the studied drugs and different proteins of the COVID-19 virus [58]. These ranking parameters are introduced below.

a) Absolute values of the Gibbs free energy of the interaction (binding) between the drug (D) and the COVID-19 protein of interest (P):

$$r_a = |\Delta G_{D-P}| = -\Delta G_{D-P} \tag{1}$$

Obviously, a more negative interaction Gibbs free energy (ΔG_{D-P}), corresponding to a stronger drug-protein interaction, gives a higher positive docking score (r_a).

b) The relative efficiency rank (scoring index) r_b defined as the ratio of the Gibbs free energy of the interaction between the drug (D) and the protein (P) of the COVID-19 virus (ΔG_{D-P}) to the Gibbs free energy of the interaction (ΔG_{D-P_r}) between the drug and a human reference protein ($P_r = ACE2$). This ranking index was calculated by Eq. (2):

$$r_b = 100 \times \left(\frac{\Delta G_{D-P}}{\Delta G_{D-P_r}}\right) \tag{2}$$

Since both Gibbs free energy values were negative, the r_b ranking index was positive. Also, it is can be said that higher ΔG_{D-P} and lower ΔG_{D-P_r} values result in higher values r_b. Obviously, drugs with larger values of r_b > 100 are more desirable.

c) The weighted sum of two differential Gibbs free energies of interactions, one between the drug and the COVID-19 protein of interest (P) and the other between the drug and the reference human protein ($P_r = ACE2$). A drug with a larger value for the former interaction and a smaller value for the latter interaction has a larger r_c value and thus is considered to be more efficient. This ranking index (r_c) was calculated by Eq. (3):

$$r_c = \alpha|(\Delta G_{D-P} - \Delta G^r_{D-P})| + \beta\left|(\Delta G_{D-P_r} - \Delta G^r_{D-P_r})\right| \tag{3}$$

In this equation, α and β are weighting factors, with the limitation $\alpha + \beta = 1$, defining the relative importance of the desired and undesired interactions. Also, the ΔG^r_{D-P} and $\Delta G^r_{D-P_r}$ parameters are the lower and upper limits (reference values) considered for the Gibbs free energies of the desired ($D-P$) and undesired ($D-P_r$) interactions, respectively. To evaluate the r_c ranking index, the following two preconditions were considered: $\Delta G_{D-P} < \Delta G^r_{D-P}$ and $\Delta G_{D-P_r} > \Delta G^r_{D-P_r}$ are. Eq. (3) denotes that higher values for the two distances, *i.e.*, $(\Delta G_{D-P} - \Delta G^r_{D-P})$ and $\left(\Delta G_{D-P_r} - \Delta G^r_{D-P_r}\right)$ distances, result in a larger value for the r_c ranking index. In the present study, $\alpha = 0.8$, $\beta = 0.2$, $\Delta G^r_{D-P_r} = -5$ kcal mol^{-1}, and $\Delta G^r_{P-D} = -7\ kcal/mol$ values were considered to evaluate the r_c ranking index to estimate the extent of the efficiency of the preferred D-P (*i.e.*, drug-COVID-19) interaction over the D-ACE2 interaction.

d) Ratio of the equilibrium constants of the binding reaction between the drug and the desired (P) and undesired (P_r) proteins, denoted by r_d , was calculated using Eq. (4):

$$r_d = \frac{K_{D-P}}{K_{D-P_r}} = \frac{exp\left(-\frac{\Delta G_{D-P}}{RT}\right)}{exp\left(-\frac{\Delta G_{D-P_r}}{RT}\right)} = exp\left[-\frac{\left(\Delta G_{D-P_r} - \Delta G_{D-P}\right)}{RT}\right] \tag{4}$$

Based on the above equation, higher (more negative) values of ΔG_{D-P} and lower (less negative) values of ΔG_{D-P_r} can result in larger values r_d ranking index. In other words, larger values of r_d, which is desirable, are obtained with more effective interactions between the drug (D) and the COVID-19 proteins $P = spike\ \&\ NSPs$ than the human protein $P_r = ACE2$.

The three r_b, r_c , and r_d ranking indices can also be considered as selectivity factors measuring the preference of the corresponding drug to interact with the desired target COVID-19 protein compared to the undesired target ACE2, as a representative human protein.

The values of the four ranking indices r_a, r_b, r_c , and r_d calculated for the interactions between the 213 screened drugs and the COVID-19 proteins and ACE2 are presented in

Tables S2-S8 (Supplementary Materials). To analyze the relatively large set of data obtained in this work, different analyses were performed and various visualizations were prepared, which are presented and discussed in the next section. It is worth noting that the interactions between the examined drugs and the Spike@ACE2 complex were found to be weak, suggesting that the drug intervention cannot occur via the drug-Spike@ACE2 interaction. Therefore, the results obtained for the drug-Spike@ACE2 docking are not presented.

RESULTS AND DISCUSSION

General Trends in Abundances

The docking scores obtained for the interaction between the studied drugs and the spike protein of the SARS-CoV-2 virus (*i.e.*, $r_a = -\Delta G_{D-S}$) are shown in Fig. 3. This drug-spike interaction and its corresponding docking score is especially important in the screening stage because of its role in the function of the virus in its initial interaction with the human cell via attachment to the ACE2 protein [57]. For the sake of comparison, the drug-ACE2 interaction Gibbs free energies ($-\Delta G_{D-ACE}$) are also plotted in Fig. 3. In this figure, the positions of clinically examined reference drugs Remdesivir [59-60] and Molnupiravir [61] in the interactions are marked with solid squares. As can be seen in Fig. 3, out of a total number of 1638 studied drugs, 305 and 464 drugs had stronger interactions with the spike protein compared to those of Remdesivir and Molnupiravir, respectively. It should be noted that the numbering scheme used for each data series in Fig. 3 (and also in Figs. S1-S10, Supplementary Materials) is based on the descending order of the drug-protein interaction free energies (ΔG_{D-P}); thus, the numbers on the horizontal axis represent the rank (score) of the drugs in the corresponding interaction.

The overall strength of the interaction between the studied drugs and the SARS-CoV-2 virus, as a whole living organism, can be estimated in terms of the average interaction energies of each drug (D) with all N_p of different proteins (P) of this virus, as shown below:

$$\Delta G_{D-Covid} = \frac{1}{N_p}\sum_{P=1}^{N_p} \Delta G_{D-P} \qquad (5)$$

where P = spike, NSP3, NSP7, NSP8, NSP9, NSP10, NSP12 (two binding sites), NSP15, NSP16, and the NSP10-NSP16 protein complex. The calculated values of ΔG_{D-COV} , which can also be considered as another docking score, are presented in Fig. 3. The average free energies were calculated for the clinically examined drugs Remdesivir [59-60] and Molnupiravir [61] and are marked in Fig. 3. As can be seen in Fig. 3, out of the 1638 drugs studied, 476 and 915 drugs had larger values of $\Delta G_{D-COVID}$, (*i.e.*, higher docking scores) than those of Remdesivir ($\Delta G_{Remdesivir-CO} = -7.4$ kcal/mol) and Molnupiravir ($\Delta G_{Molnupiravir-COVID} = -6.5$ kcal/mol), respectively.

A comparative analysis of $-\Delta G_{D-Spi}$ and $-\Delta G_{D-COV}$ curves in Fig. 3 showed that the number of drugs having stronger interactions with NSP proteins, compared to that of remdesivir and molnupiravir, was larger than that of the spike. This suggests that by exposing the virus to a wider range of drugs via a cocktail, it can be inhibited not only at the stage before entering the cell (*i.e.*, attachment of the coronavirus spike protein to the ACE2 protein) but also at other stages, including SARS-CoV2 entry, membrane fusion, RNA release, translation, and RNA replication inside the cell. Also, Fig. 3 shows that among the examined drugs, the ranking of molnupiravir in terms of averaged interactions with COVID-19 NSP proteins is lower than that with the

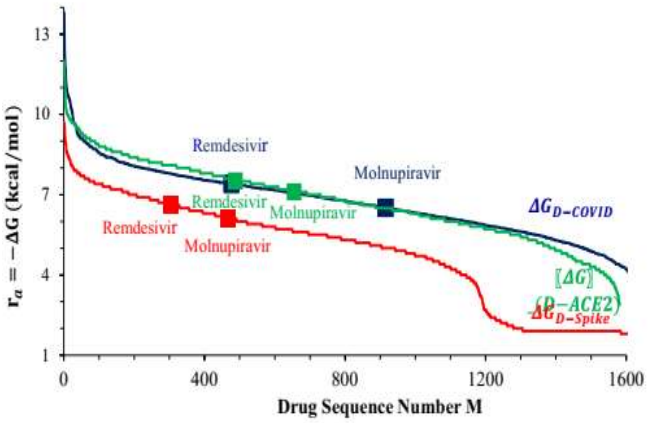

Fig. 3. The drug-spike (D-Spike) and drug-ACE2 (D-ACE2) docking scores (r_a) and the average drug-COVID interaction Gibbs free energy obtained in the present docking study for the 1638 approved drugs. The colored squares mark the corresponding values for the clinically examined drugs Remdesivir and Molnupiravir (color online).

ACE2 protein. The trends of the D-P interaction Gibbs free energies for other proteins of COVID-19 virus were visualized and are presented in Figs. S1-S10 (Supplementary Materials). It must be added that in Fig. 3 and Figs. S1-S10, each data set is plotted in the descending order of the corresponding drug-protein interaction energies; therefore, the sequence number for each drug in different interaction energies (representing its corresponding docking score) is different. As a result, a given drug sequence number on the horizontal axis may not necessarily point to an identical drug for different drug-protein interactions.

An abundance analysis was carried out on the docking scores r_a (Gibbs free energies) obtained for the D-Spike, D-ACE2, and D-COVID interactions presented in Fig. 3, with a summation width of 0.4 kcal mol^{-1} and an increment of 0.2 kcal mol^{-1}. The results of this abundance analysis are illustrated in Fig. 4. The peak appearing in the middle of the abundance curves in Fig. 4 corresponds to the flatter (lower slope) part of the affinities in Fig. 3. It can be seen from Fig. 4 that in the range of 6-8 kcal mol^{-1} interaction Gibbs free energies, the number of drugs affecting the desired target (*i.e.*, COVID-19 proteins) was larger than that affecting the undesired target (*i.e.*, the human protein ACE2). Therefore, the common drugs located in this region of the two abundance curves can be considered as selective drugs for the treatment of COVID-19. Similar to what was inferred from Fig. 3, a comparative analysis of the two abundance curves of the drug-COVID and drug-Spike interactions in Fig. 4 showed that the drug-NSPs interactions were generally stronger than the drug-spike interactions. It can be seen more clearly from Fig. 4 that the number of drugs with stronger drug-COVID-19 and drug-spike interactions was more than those of the two clinically examined reference drugs Remdesivir and molnupiravir.

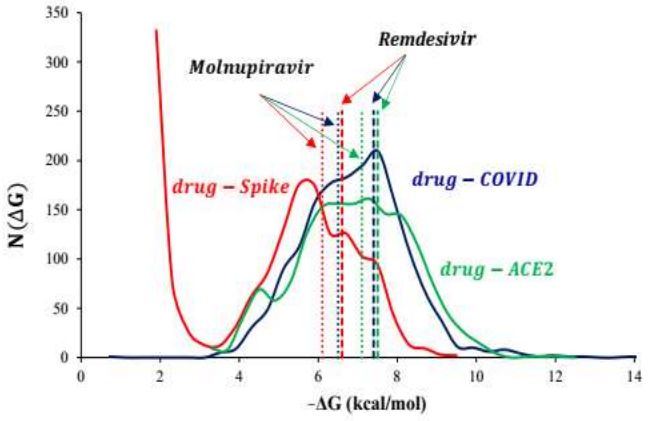

Fig. 4. Abundances N(ΔG), derived for the drug-spike ($\Delta G_{D-Spike}$), drug-ACE2 (ΔG_{D-ACE2}), and the average drug-COVID (ΔG_{D-COV} , Eq. (5)) interaction Gibbs free energies (affinities) presented in Fig. 3. The corresponding values for the clinically examined Remdesivir and Molnupiravir drugs are marked with the dashed and dotted vertical lines in the same corresponding colors, respectively (color online).

Ranking the Approved Drugs

The Gibbs free energies obtained for the interactions between the 213 screened drugs and the COVID-19 (spike and NSPs) and the human ACE2 proteins, as well as the calculated values of the four ranking indices r_a, r_b, r_c, and r_d introduced in Eqs. ((1)-(4)) in Section 2.3.2, are listed in Tables S2-S8 (Supplementary Materials). A short list of the drugs scored highest in their interactions with the COVID-19 proteins and the human ACE2 protein based on each of the four ranking indices is presented in Table 1. For example, as can be seen in this Table, among the examined drugs, Cidofovir ($C_8H_{14}N_3O_6P$), fosamprenavir ($C_{25}H_{36}N_3O_9PS$), and vitamin E ($C_{29}H_{50}O_2$) had the highest ranking, respectively, based on the ratio of the Gibbs free energies (r_b) of the drug-spike and drug-ACE2 interactions. Details of the interactions between the first three highest-ranked drugs (Table 1) and the spike and NSP7 proteins of COVID-19 and the human ACE2 protein are presented in Figs. 5, 6, and 7, respectively. Details of the interactions between a larger list (Fig. S11) of highest-ranked drugs for each protein are shown in Figs. S12, S13, and S14 (Supplementary Materials), respectively. The absolute values of the interaction (binding) Gibbs free energies for the three highest-ranked drugs fell in the ranges of 9.19-9.74, 6.1-6.44, and 8.91-9.82 kcal mol^{-1} for the spike, NSP7, and ACE2 proteins, respectively. Also, as another example, vitamin E ranked third based on the efficiency ranking index r_b in its interaction with spike, for which the free energies of interaction with spike and ACE2 proteins were -6.49 and -4.11 kcal mol^{-1}, respectively. The binding mode and key interactions between the target proteins and the drugs standing highest based on the four ranking indices, corresponding to the most stable positions and conformations of the ligands, were determined and

Table 1. The First 12 Drugs Ranked Highest in Their Interactions with Different Proteins of the SARS-CoV-2 Virus Based on the Present Molecular Docking Study

rank	Spike				NSP3				NSP7				NSP8			
	r_a	r_b	r_c	r_d	r_a	r_b	r_c	r_d	r_a	r_b	r_c	r_d	r_a	r_b	r_c	r_d
1	1376	390	626	438	1376	226	862	663	1297	1355	1297	1355	604	391	604	391
2	626	438	612	609	1297	663	1376	402	1376	613	591	437	626	211	609	681
3	862	969	1376	969	862	761	641	761	190	617	190	613	741	681	626	211
4	612	226	862	620	388	412	573	1333	591	412	1355	412	416	613	467	366
5	515	1483	1499	756	626	402	388	437	266	437	1376	226	388	437	391	437
6	1499	1003	609	958	573	1333	402	434	836	641	266	617	467	327	416	613
7	1538	756	1538	717	266	437	1297	1224	592	28	592	366	609	434	388	1483
8	1297	412	515	1499	641	1003	609	641	331	150	331	430	1297	604	741	327
9	609	761	739	681	416	434	1154	466	736	573	573	231	1376	609	613	434
10	416	437	416	754	736	390	626	412	515	276	617	28	1484	150	1484	1299
11	736	430	620	390	609	1224	416	1626	603	430	467	1483	603	517	211	1626
12	739	620	604	437	592	1483	266	1154	573	753	603	1626	331	1355	603	517

rank	NSP9				NSP10				NSP12				NSP12 (R)			
	r_a	r_b	r_c	r_d	r_a	r_a	r_b	r_c	r_d	r_a	r_a	r_b	r_c	r_d	r_a	r_a
1	467	226	467	437	391	331	1297	226	1297	226	641	391	331	1297	226	641
2	609	412	609	753	681	1147	641	641	641	641	629	681	1147	641	641	629
3	1497	437	1497	616	211	573	1376	1003	1376	1003	1297	211	573	1376	1003	1297
4	604	1003	604	276	366	190	629	1483	629	1483	1484	366	190	629	1483	1484
5	736	1483	641	517	437	592	467	1333	467	1333	467	437	592	467	1333	467
6	416	1299	753	609	613	615	1484	412	1484	412	1376	613	615	1484	412	1376
7	641	753	736	1626	1483	1297	626	761	626	761	626	1483	1297	626	761	626
8	741	61	616	97	327	617	331	969	331	969	615	327	617	331	969	615
9	590	616	1499	412	434	591	615	434	615	434	331	434	591	615	434	331
10	388	1626	416	958	1299	612	388	391	388	391	1499	1299	612	388	391	1499
11	515	97	388	641	1626	1484	416	437	416	437	609	1626	1484	416	437	609
12	739	276	739	1642	517	467	1499	138	1499	138	388	517	467	1499	138	388

rank	NSP15				NSP16				NSP10-NSP16				ACE2
	r_d	r_a	r_a	r_b	r_c	r_d	r_a	r_a	r_b	r_c	r_d	r_a	r_a
1	1297	226	1297	558	641	391	331	1297	226	641	391	331	1376
2	1376	1483	190	327	629	681	1147	641	641	629	681	1147	836
3	190	1003	558	1003	1297	211	573	1376	1003	1297	211	573	1297
4	266	703	1376	701	1484	366	190	629	1483	1484	366	190	741
5	1499	558	1499	969	467	437	592	467	1333	467	437	592	190
6	592	327	592	226	1376	613	615	1484	412	1376	613	615	515
7	558	969	604	1499	626	1483	1297	626	761	626	1483	1297	398
8	1549	1642	266	1642	615	327	617	331	969	615	327	617	742
9	604	701	1549	1483	331	434	591	615	434	331	434	591	1298
10	739	663	739	663	1499	1299	612	388	391	1499	1299	612	266
11	591	438	701	654	609	1626	1484	416	437	609	1626	1484	736
12	836	434	591	434	388	517	467	1499	138	388	517	467	590

Note. The drugs ranked highest in their interactions with the human ACE2 protein (as a reference) are also presented in the table. The numbers in this table refer to the drug numbers introduced in Tables S2-S8 (Supplementary Materials).

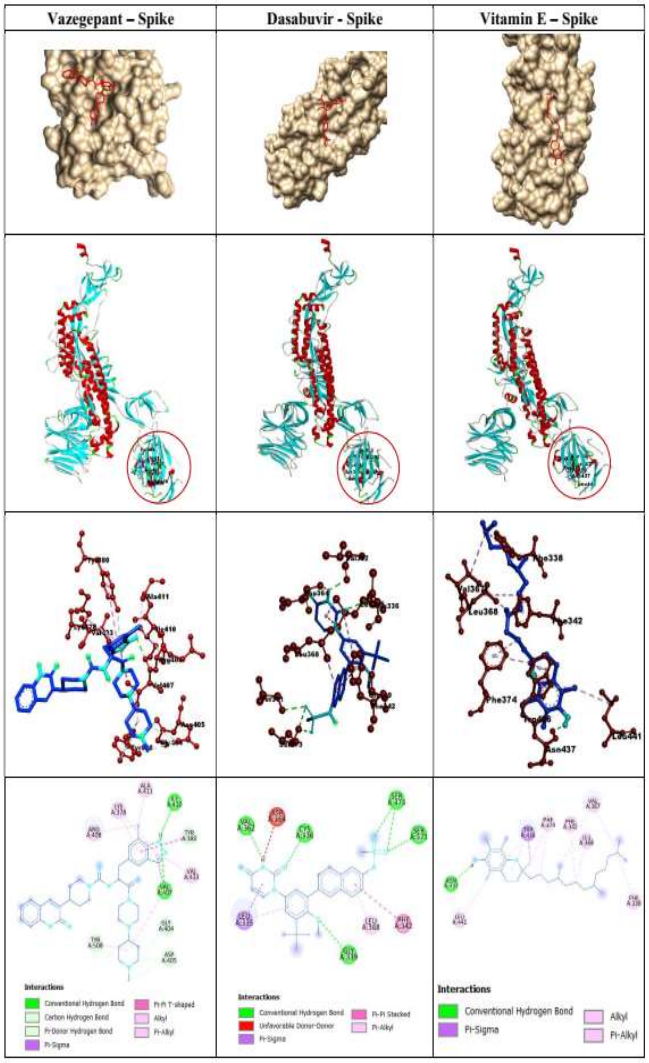

Fig. 5. Details of the ligand-protein interactions for the selected ligands having the highest docking scores (ranking indices) in their interactions with the spike protein of SARS-CoV-2 virus. Only the most important amino acid residues are shown (color online).

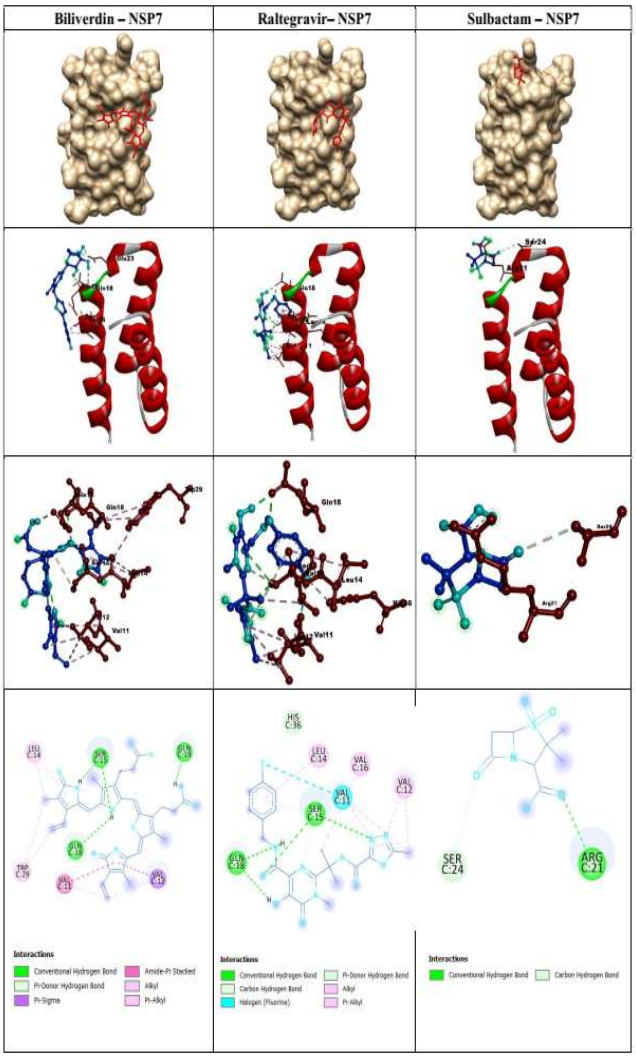

Fig. 6. Details of the ligand-protein interactions for the selected ligands having the highest docking scores (ranking indices) in their interactions with the NSP7 protein of COVID-19 (color online).

analyzed. The structures of these drugs are shown in Fig. S11, and their intermolecular interactions with the amino acid residues of the spike, NSP7 (as a representative NSP), and ACE2 proteins are visualized in Figs. S12, S13, and S14, respectively. Details of the drug-protein interactions between the three highest-ranked drugs and spike, NSP7, and ACE2 proteins are presented in Figs. 5, 6, and 7, respectively. These visualizations were prepared using the BioVia Discovery Studio Client [62] and Chimera software [63].

Details of the Drug-Protein Interactions

The general positions of the ligands (drugs) in the binding pocket of the spike protein of COVID-19 are displayed in the first row of each panel of Fig. 5, in which the ligands are illustrated by the red stick model and the spike protein residues are shown by the merged atomic surfaces. In addition, the dockings of the ligands into the spike binding

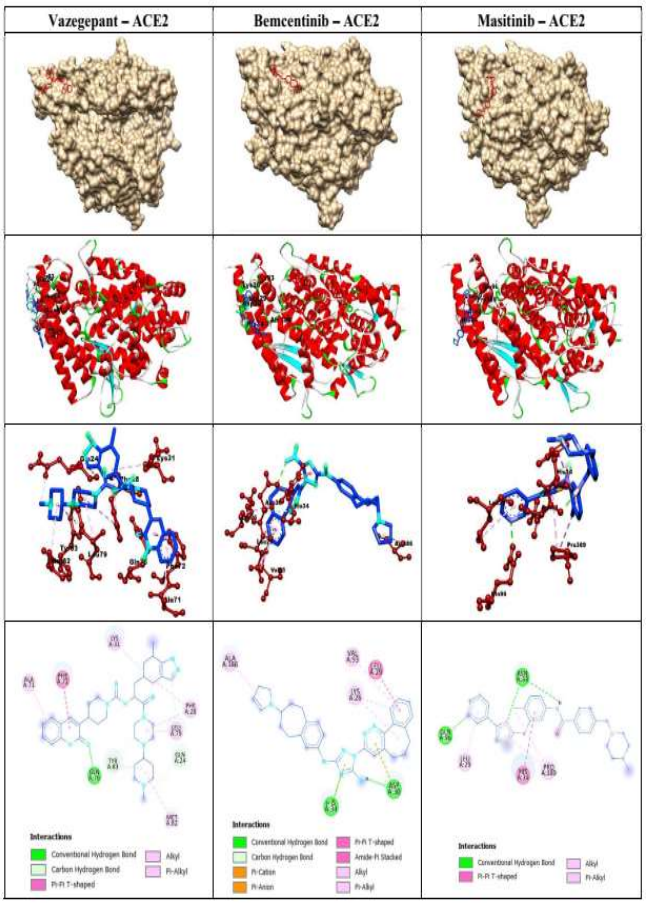

Fig. 7. Details of the ligand-protein interactions for the selected ligands having the highest docking scores (ranking indices) in their interactions with ACE2, as the reference human protein (Color online).

pocket are presented in the second row of Fig. 5, but with emphasis on the fourth structure of the protein. The amino acids (ball and stick models of crimson colors), surrounding the ligands (the blue stick model) in the binding pocket of the spike protein, and their corresponding interactions (the dashed lines) in the three- and two-dimensional presentations are shown in the third and fourth rows of Fig. 5, respectively. The same illustration style and order were used for the drug-NSP7 and drug-ACE2 interactions, presented in Figs. 6 and 7, respectively.

In the present study, the most effective interactions between vazegepant and COVID-19 spike glycoprotein in the spike-ACE2 binding region obtained consisted of the following:

1) Two N−H···O=C hydrogen bond interactions between the vazegepant indazole ring N-H hydrogen atom and the oxygen atom of the carbonyl groups of Val 407 and Ile 410 amino acids,

2) Several pi-alkyl (π···H−C) interactions between the π-bond of the indazole ring of this drug and the C−H bond of the Val 433 and Lys 378 residues,

3) π-donor hydrogen bond interactions between the C−H bond of the drug and the π electrons of the carbonyl groups of Asp 405 and Gly 404, and

4) Unconventional carbon-hydrogen bond (C−H···O) interactions between the C−H bond of vazegepant and the hydroxyl group oxygen atom of Tyr 508 residue.

The analysis of the dasabuvir-spike docking results showed the promising inhibition of this protein by dasabuvir. As shown in Fig. 5, this inhibition was due to the four significant hydrogen bond interactions, which can be categorized into the following three groups: *1*) the (N−H···O=C) hydrogen bond between the N−H hydrogen atom of dasabuvir pyrimidine-2,4-dione ring and the oxygen atom of the carbonyl groups of the Val 362 and Cys 336 residues, 2) the ((CH_3-)(Phen−)O···H−N) hydrogen bond between the oxygen atom of the methoxy substitution on the phenyl ring (Phen) of the drug and the N−H hydrogen atom of the Gly 339 residue, and 3) the ((Napht−NH−)$(CH_3-)SO_2$···H−O) hydrogen bond between the oxygen atoms of the drug methanesulfonamide (Napht−NH−SO_2−CH_3) group and the O−H hydrogen atoms of the Ser 371 and Ser 373 residues. Furthermore, the dasabuvir-spike binding included pi-pi (π···π), pi-alkyl (π···H−C), and pi-sigma (π···[C−H]) interactions, between the dasabuvir naphthalene ring and the Phe 342 phenyl ring and the Leu 368 isopropyl group, and between the drug pyrimidine-2,4-dione ring and the Leu 335 isopropyl group sigma bonds, respectively.

The other drug that showed high affinity (-6.49 kcal mol^{-1}) toward the COVID-19 spike protein was vitamin E, which has been considered as the base medication in the treatment of all COVID-19 in- and out-patients across the world [64-65]. As can be seen in Fig. 5, the vitamin E-spike interaction consisted of three major sets of interactions, including a hydrogen bond between the hydrogen atom of the chromane (3,4-dihydro-2*H*-1-benzopyran) hydroxyl group of

vitamin E and the oxygen atoms of the Asn 437 residue, the sigma-pi interactions between the methyl substitutions on the chromane ring of vitamin E and the aromatic indole ring of Trp 436 amino acid, and various alkyl-pi interactions between the C−H bonds of the drug methyl, methylene, and isopropyl groups and the aromatic phenyl ring of the Phe 374, 342, and 338 residues.

Based on the ranking indices r_b and r_d, biliverdin was ranked first concerning the interaction with the COVID-19 NSP7 protein. As shown in Fig. 6, its interaction with NSP7 included four hydrogen bonds, of which two were between the N−H hydrogen atom of the drug pyrazole ring with the oxygen atoms of the carbonyl group of the Gln 18 and the amide functional group of the Ser 15 residue, the third was between the N−H hydrogen atom of 3-methyl-4,5-divinyl-1,5-dihydro-2H-pyrrol-2-one of biliverdin and the O−H oxygen atom of Ser 15, and the fourth was between the drug carboxylic acid hydrogen atom and the oxygen atom belonging to the amide group of Gln 19. Also, significant amide-pi stacked and pi-sigma interactions were observed between the 4-methyl-3,5-divinyl-2H-pyrrol-2-one moiety of the drug and Val 11 and Val 12 residues. The results of the molecular docking performed for the biliverdin-NSP7 drug-protein system also showed several pi-alkyl interactions. The first pi-alkyl interaction was established between the methyl group vicinal to the carbonyl and vinyl substituents of biliverdin and the pi electrons of the indole ring of Trp 29, the second between the pi electrons of the end ring having methyl group vicinal to the carbonyl substitution and isopropyl group hydrogen atoms of Leu 14, and the third between the pi electrons of the other end ring with the vicinal carbonyl and vinyl groups of the drug and the isopropyl group hydrogen atoms of Val 11 and Val 12 residues.

The major raltegravir-NSP7 interaction (Fig. 6) can be attributed to the formation of four hydrogen bonds. Two of these hydrogen bonds were formed between the hydrogen atoms of the hydroxyl and amide groups attached to the pyrimidine ring of the raltegravir molecule and the oxygen atom of the carbonyl group of Gln 18 residue, and the other two hydrogen bonds were formed between the oxadiazole ring nitrogen and the pyrimidine ring carbonyl oxygen atoms of the drug, on the one hand, and the O−H hydrogen atom of the Ser 15 amino acid, on the other hand. In the raltegravir-NSP7 interaction, the fluorine atom also played a role by participating in the interaction between weak F···H−C(imidazole) unconventional hydrogen bond and the F···π*(carbonyl), on the one hand, and the Val 11 residue, on the other hand. Furthermore, raltegravir and NSP7 were also engaged via the pi-alkyl interactions between the drug phenyl and oxadiazole rings, on the one hand, and the isopropyl groups of the Leu 14 and Val 12 amino acids of the NSP7 protein, on the other hand, respectively.

The most important interactions involved in the sulbactam-NSP7 protein binding (Fig. 6) were the (C=O···H−N) hydrogen bond between the carbonyl oxygen atom of the drug carboxylic acid group and the N−H hydrogen atom of the Arg 21 residue, and the (C=O···H−O−CH_2−) hydrogen bond between the drug beta-lactam carbonyl group oxygen atom and the −CH_2−OH hydrogen atom of the Ser 24 residue.

The results of this docking study regarding the interaction between vazegepant and COVID-19 NSP7 protein led to the identification of three hydrogen bond interactions (Fig. S13). Two of these hydrogen bonds were (C=O···H−O) and (N···H−O) formed between the drug carbonyl oxygen and piperazine ring nitrogen atoms, on the one hand, and the hydroxyl group hydrogen atom in the Ser 15 residue, on the other hand. The third hydrogen bond (N−H···O=C) was formed between the quinolin-2(1H)-one N−H hydrogen atom of vazegepant and the carbonyl oxygen atom of the Cys 8 residue. The pi-sigma (π···[C−H]) and pi-alkyl (π···C−H) interactions between different π orbitals of the drug and the C−H bonds of the Gln 19, Val 12, Val16, Val12, and Trp 29 residues were also involved in the vazegepant-NSP7 interaction. In addition, two (C−H···O=C) unconventional hydrogen bonds were observed between the C−H bonds of the indazole and the piperazine rings of the drug, on the one hand, and the carbonyl oxygen atoms of the Val 12 and Ser 15 amino acids, on the other hand.

Furthermore, vazegepant displayed a strong affinity (−9.82 kcal mol^{-1}) toward the human ACE2 glycoprotein. The vazegepant-ACE2 interaction (Fig. 7) involved the following: 1) a (C=O···H−O) hydrogen bond between the carbonyl oxygen atom of the drug lactam ring and the amide N−H hydrogen atom of the Gln 76 residue, 2) a pi-pi (π···π) interaction between the aromatic quinoline ring of the drug and the phenyl ring of the Phe 72 residue, 3) two pi-alkyl (π···H−C) interactions, one between the vazegepant

quinoline phenyl ring and the C-H bond of the methyl group of Ala 71 residue and the other between the C−H bond of the drug piperazine and the phenyl ring of Phe 28, and 4) two sets of carbon-hydrogen bond interactions, one (C−H⋯ O=C) between the C-H bonds of pyrazole ring and the methyl substituent of 1-methyl piperidine moiety with the oxygen atoms of the amide functional groups of Gln 24 and the other (C−H⋯O−phen) between piperazine C−H bonds of the drug and the phenol ring oxygen atom of the Tyr 83 residue.

The drug named masitinib also showed high affinity (with a binding energy of −9.04 kcal mol^{-1}) toward the ACE2-human glycoprotein (Fig. 7). The strong masitinib-ACE2 interaction can be attributed primarily to the three hydrogen bond interactions, including 1) one between the nitrogen atom of the pyridine ring in masitinib and the oxygen atom of the amide functional group of Gln 96, 2) one between the hydrogen atom of the amide group attached to the phenyl ring in the drug and the oxygen atom of the carbonyl group of Asn 33, and 3) one between the nitrogen atom of the drug thiazole ring and the hydrogen atom of the amide group of Asn 33 amino acid. In addition, masitinib had pi-pi and pi-alkyl interactions with the His 34, Leu 29, and Pro 389 residues of ACE2.

As the last example of the drug-protein interactions derived from the present molecular docking study, the bemcentinib-ACE2 interaction is analyzed below. The results showed that there were two hydrogen bonds (Fig. 7), one between the N-H hydrogen atom of the only amine group of bemcentinib (attached to the thiazole ring) and the oxygen atom of the amide functional group of Asp 30, and the other between the sp^2 nitrogen atom of the triazole ring of bemcentinib and the N-H (of imidazole ring) hydrogen atom of His 34 residue. The pi-pi interaction between the drug π-systems and the carbonlyl π bond of Leu 29, pi-alkyl, and carbon-hydrogen bond interactions, on the one hand, and Val 93, Lys 26, Ala 386, and Asp 30 residues, on the other hand, also contributed to the bemcentinib-ACE2 binding.

CONCLUSIONS

A virtual screening molecular docking approach was used to identify some potential inhibitors among 1638 approved drugs against COVID-19 proteins. For this purpose, the interactions between these drugs and the SARS-CoV-2 virus proteins, including spike and non-structural proteins NSP3, NSP7, NSP8, NSP9, NSP10, NSP12, NSP15, NSP16, and the NSP10-NSP16 complex, were evaluated. Also, the dockings of these approved drugs on the human ACE2 protein, as a reference protein, and its complex with the spike (Spike@ACE2) were investigated. The virtual screening was carried out in two stages, and the results were evaluated based on four ranking indices (docking scores) used to measure the comparative strengths of drug-protein binding interactions (affinities). In the first stage, molecular docking was carried out and the ratio of the Gibbs free energies (r_b) interaction between the drug-protein (COVID-19) and drug-ACE2 (human) complexes were calculated and used to rank the interaction between each drug and each COVID-19 protein. At this stage, the highest-ranked 50 drugs in the 11 ranking lists were obtained based on the r_b index for all COVID-19 proteins and collected in a list of 213 drugs for the next stage, in which a complete docking procedure was used to re-evaluate the interaction energies and rankings with higher accuracy. Collective analysis of all calculated affinities, presented for the first time in this study, revealed interesting trends for the sensitivity of the SARS-CoV-2 virus, as a whole, toward the examined drugs. Details of the drug-protein interactions were derived, visualized, and discussed for some drugs having the highest ability to inhibit the spike, NSP7, and ACE2 representative proteins. Based on the results of this docking study, vazegepant, dasabuvir, vitamin E, fosamprenavir, raltegravir, canagliflozin, biliverdin, and imatinib approved drugs, which ranked highest in their interactions with the COVID-19 proteins, are proposed as promising candidates for further computational and experimental studies required in the final screening stage to be repurposed as medication against COVID-19 disease. Furthermore, the results showed that a significant number of drugs had stronger interactions with the spike protein and displayed larger average Gibbs free energy of interaction with the SARS-CoV-2 virus compared to clinically examined reference drugs remdesivir and molnupiravir. Also, the analysis of the abundance curves showed that the number of drugs having strong interactions with NSP proteins was more than those having strong interactions with spike. Therefore, in addition to spike, the NSP proteins should also be considered in the effective treatment of COVID-19.

According to the results obtained in this study, different

proteins contribute to the SARS-CoV-2 virus replication cycle at different stages, and for each protein, there may exist specific drugs that have the strongest interactions (inhibitory effect). Thus, upon the completion of the last stage of the screening study, a cocktail therapy or any other synergistic drug combination schemes can be proposed for the inhibition of the SARS-CoV-2 virus by using two or more drugs screened at the final stage.

ACKNOWLEDGMENTS

The authors gratefully acknowledge Mr. M. R. Torabi for his assistance in handling a large body of data using appropriate software packages.

REFERENCES

[1] World Health Organization, "Timeline-WHO's COVID-19 response", reported in https://covid19.who.int/, accessed on 2022/10/21.

[2] Xiao, J.; Fang, M.; Chen, Q.; He, B., SARS, MERS and COVID-19 Among Healthcare Workers: A Narrative Review. *J. Infect. Pub. Health*, **2020**, *13* (6), 843-848, DOI: 10.1016/j.jiph.2020.05.019.

[3] Boopathi, S.; Poma, A. B.; Kolandaivel, P., Novel 2019 Coronavirus Structure, Mechanism of Action, Antiviral Drug Promises and Rule out Against Its Treatment. *J. Biomol. Struct. Dyn.* **2020**, *39* (9), 3409-3418, DOI: 10.1080/07391102.2020.1758788.

[4] Shin, D.; Mukherjee, R.; Grewe, D.; Bojkova, D.; Baek, K.; Bhattacharya, A.; Schulz, L.; Widera, M.; Mehdipour, A. R.; Tascher, G.; Geurink, P. P., Papain-like Protease Regulates SARS-CoV-2 Viral Spread and Innate Immunity. *Nature* **2020**, *587* (7835), 657-662, DOI: doi.org/10.1038/s41586-020-2601-5.

[5] Andrade, B. S.; Rangel. F. D. S.; Santos, N. O., *et al*., Repurposing Approved Drugs for Guiding COVID-19 Prophylaxis: A Systematic Review. *Front. Pharmacol*. **2020**, *11*, 590598, DOI: 10.3389/fphar.2020.590598.

[6] Rocca, E.; Gauffin, O.; Savage, R.; Vidlin, S. H.; Grundmark, B., Remdesivir in the COVID-19 Pandemic: An Analysis of Spontaneous Reports in VigiBase During 2020. *Drug Saf*. **2021**, *44* (9), 987-998, DOI: 10.1007/s40264-021-01091-x.

[7] ACTT-1 Study Group., Remdesivir for the Treatment of Covid-19: Final Report. *N. Engl. J. Med.* **2020**, *383* (19), 1813-1826, DOI:10.1056/NEJMoa2007764.

[8] Stromgaard, K.; Krogsgaard-Larsen, P., Madsen, U. *Textbook of Drug Design and Discovery*; CRC (Talor & Francis) **2009**, p. 1-467.

[9] Talluri, S., Virtual Screening Based Prediction of Potential Drugs for COVID-19. *Comb. Chem. High Throughput Screen.* **2021**, *24*, 716-728, DOI: 10.2174/1386207323666200814132149.

[10] Nogara, P. A.; Omage, F. B.; Bolzan, G. R.; Delgado, C. P.; Orian, L.; Rocha, J. B. T., Reactivity and Binding Mode of Disulfiram, Its Metabolites, And Derivatives in SARS-CoV-2 PLpro: Insights from Computational Chemistry Studies. *J. Mol. Model.* **2022***, 28* (11), 1-12, DOI: 10.1007/s00894-022-05341-2.

[11] Shree, P.; Mishra, P.; Selvaraj, C.; Singh, S. K.; Chaube, R.; Garg, N.; Tripathi, Y. B., Targeting COVID-19 (SARS-CoV-2) Main Protease Through Active Phytochemicals of Ayurvedic Medicinal Plants-Withania Somnifera (Ashwagandha), Tinospora Cordifolia (Giloy) and Ocimum Sanctum (Tulsi)-A Molecular Docking Study. *J. Biomol. Struct. Dyn.* **2022**, *40* (1), 190-203, DOI: 10.1080/07391102.2020.1810778.

[12] Khelfaoui, H.; Harkati, D.; Saleh, B. A., Molecular Docking, Molecular Dynamics Simulations and Reactivity, Studies on Approved Drugs Library Targeting ACE2 and SARS-CoV-2 Binding with ACE2. *J. Biomol. Struct. Dyn.* **2021**, *39* (18), 7246-7262, DOI: 10.1080/07391102.2020.1803967.

[13] Joshi, T.; Joshi, T.; Pundir, H.; Sharma, P.; Mathpal, S.; Chandra, S., Predictive Modeling by Deep Learning, Virtual Screening and Molecular Dynamics Study of Natural Compounds Against SARS-CoV-2 Main Protease. *J. Biomol. Struct. Dyn.* **2021**, *39* (17), 6728-6746, DOI: 10.1080/07391102.2020.1802341.

[14] Alazmi, M.; Motwalli, O., *In Silico* Virtual Screening, Characterization, Docking and Molecular Dynamics Studies of Crucial SARS-CoV-2 Proteins. *J. Biomol. Struct. Dyn.* **2021**, *39* (17), 6761-6771, DOI: 10.1080/07391102.2020.1803965.

[15] Ghosh, R.; Chakraborty, A.; Biswas, A., Chowdhuri, S., Evaluation of Green Tea Polyphenols as Novel

Corona Virus (SARS CoV-2) Main Protease (Mpro) Inhibitors-An *In Silico* Docking and Molecular Dynamics Simulation Study. *J. Biomol. Struct. Dyn.* **2021**, *39* (12), 6747-6760, DOI: 10.1080/07391102.2020.1802347.

[16] Hosseini, F. S.; Amanlou, M., Anti-HCV and Anti-malaria Agent, Potential Candidates to Repurpose for Coronavirus Infection: Virtual Screening, Molecular Docking, and Molecular Dynamics Simulation Study. *Life Sci*. **2020**, *258*, 118205, DOI: 10.1016/j.lfs.2020.118205.

[17] Kapusta, K.; Kar, S.; Collins, J. T., *et al*., Protein Reliability Analysis and Virtual Screening of Natural Inhibitors for SARS-CoV-2 Main Protease (Mpro) Through Docking, Molecular Mechanic & Dynamic, and ADMET Profiling. *J. Biomol. Struct. Dyn.* **2021**, *39* (17), 6810-6827, DOI: 10.1080/07391102.2020.1806930.

[18] Garg, S.; Anand, A.; Lamba, Y.; Roy, A., Molecular Docking Analysis of Selected Phytochemicals Against SARS-CoV-2 Mpro Receptor. *Vegetos*. **2020**, *33* (4), 766-781, DOI: 10.1007/s42535-020-00162-1.

[19] Keretsu, S.; Bhujbal, S. P.; Cho, S. J., Rational Approach Toward COVID-19 Main Protease Inhibitors *Via* Molecular Docking, Molecular Dynamics Simulation and Free Energy Calculation. *Sci. Rep.* **2020**, *10* (1), 17716, DOI: 10.1038/s41598-020-74468-0.

[20] Basu, A.; Sarkar, A.; Maulik, U., Molecular Docking Study of Potential Phytochemicals and Their Effects on the Complex of SARS-CoV2 Spike Protein and Human ACE2. *Sci. Rep.* **2020**, *10*, 17699, DOI: 10.1038/s41598-020-74715-4.

[21] Alnajjar, R.; Mostafa, A.; Kandeil, A.; Al-Karmalawy, A. A., Molecular Docking, Molecular Dynamics, and In Vitro Studies Reveal the Potential of Angiotensin II Receptor Blockers to Inhibit the COVID-19 Main Protease. *Heliyon*. **2020**, *6* (12), e05641, DOI: 10.1016/j.heliyon.2020.e05641.

[22] El-Hawary, S. S.; Rabeh, M. A.; Raey, M. A. E., *et al*., Metabolomic Profiling of Three Araucaria Species, and Their Possible Potential Role Against COVID-19. *J. Biomol. Struct. Dyn.* **2021**, in press, DOI: 10.1080/07391102.2021.1885494.

[23] Mahmud, S.; Biswas, S.; Paul, G. K., *et al*., Antiviral Peptides Against the Main Protease of SARS-CoV-2: A Molecular Docking and Dynamics Study. *Arab. J. Chem.* **2021**, *14*, 103315, DOI: 10.1016/j.arabjc.2021.103315.

[24] Khatabi, K. E.; Aanouz, I.; Alaqarbeh, M.; Ajana, M. A.; Lakhlifi, T.; Bouachrine, M., Molecular Docking, Molecular Dynamics Simulation, and ADMET Analysis of Levamisole Derivatives Against the SARS-CoV-2 Main Protease (Mpro). *BioImpacts: BI* **2022**, *12* (2), 107, DOI: 10.34172/bi.2021.22143.

[25] Belhassan, A.; Zaki, H.; Chtita, S.; Alaqarbeh, M.; Alsakhen, N.; Benlyas, M.; Lakhlifi, T.; Bouachrine, M., Camphor, Artemisinin and Sumac Phytochemicals as Inhibitors Against COVID-19: Computational Approach. *Comput. Biol. Med.* **2021**, *136*, 104758, DOI: 10.1016/j.compbiomed.2021.104758.

[26] Iftikhar, H.; Ali, H. N.; Farooq, S.; Naveed, H.; Shahzad-ul-Hussan, S., Identification of Potential Inhibitors of Three Key Enzymes of SARS-CoV2 Using Computational Approach. *Comput. Biol. Med.* **2020**, *122*, 103848, DOI: 10.1016/j.compbiomed.2020.103848.

[27] Rao, P.; Shukla, A.; Parmar, P., *et al*., Reckoning A Fungal Metabolite, Pyranonigrin A as A Potential Main Protease (Mpro) Inhibitor of Novel SARS-CoV-2 Virus Identified Using Docking and Molecular Dynamics Simulation. *Biophys. Chem.* **2020**, *264*, 106425, DOI: 10.1016/j.bpc.2020.106425.

[28] Tripathi, M. K.; Singh, P.; Sharma, S.; Singh, T. P.; Ethayathulla, A. S.; Kaur, P., Identification of Bioactive Molecule from Withania Somnifera (Ashwagandha) as SARS-CoV-2 Main Protease Inhibitor. *J. Biomol. Struct. Dyn.* **2021**, *39* (15), 5668-5681, DOI: 10.1080/07391102.2020.1790425.

[29] Bharadwaj, S.; Lee, K. E.; Dwivedi, V. D.; Kang, S. G., Computational Insights Into Tetracyclines as Inhibitors Against SARS-CoV-2 Mpro *Via* Combinatorial Molecular Simulation Calculations. *Life Sci.* **2020**, *257*, 118080, DOI: 10.1016/j.lfs.2020.118080.

[30] de Lima Menezes, G.; da Silva, R. A.,Identification of Potential Drugs Against SARS-CoV-2 Non-structural Protein 1 (NSP1). *J. Biomol. Struct. Dyn.* **2021**, *39* (15), 5657-5667, DOI: 10.1080/07391102.2020.1792992.

[31] Andrianov, A. M.; Kornoushenko, Y. V.; Karpenko, A. D.; Bosko, I. P.; Tuzikov, A. V., Application of Deep Learning and Molecular Modeling to Identify Small Drug-like Compounds as Potential HIV-1 Entry Inhibitors. *J. Biomol. Struct. Dyn.* **2021**, *39*, 5779-5791, DOI: 10.1080/07391102.2020.1792989.

[32] Mishra, S. S.; Ranjan, S.; Sharma, C. S.; Singh, H. P.; Kalra, S.; Kumar, N., Computational Investigation of Potential Inhibitors of Novel Coronavirus 2019 Through Structure-based Virtual Screening, Molecular Dynamics and Density Functional Theory Studies. *J. Biomol. Struct. Dyn.* **2021**, *39* (12), 4449-4461, DOI: 10.1080/07391102.2020.1791957.

[33] Rahman, M. M.; Saha, T.; Islam, K. J.; Suman, R. H.; Biswas, S.; Rahat, E. U.; Halim, M. A., Virtual Screening, Molecular Dynamics and Structure-activity Relationship Studies to Identify Potent Approved Drugs for Covid-19 Treatment. *J. Biomol. Struct. Dyn.* **2021**, *39* (16), 6231-6241, DOI: 10.1080/07391102.2020.1794974.

[34] Gulotta, M. R.; Lombino, J.; Perricone, U., *et al*., Targeting SARS-CoV-2 RBD Interface: A Supervised Computational Data-driven Approach to Identify Potential Modulators. *Chem. Med. Chem.* **2020**, *15* (20), 1921-1931, DOI: 10.1002/cmdc.202000259.

[35] Alajmi, M. F.; Azhar, A.; Owais, M., *et al*., Antiviral Potential of Some Novel Structural Analogs of Standard Drugs Repurposed for the Treatment of COVID-19. *J. Biomol. Struct. Dyn.* **2021**, *39* (17), 6676-6688, DOI: 10.1080/07391102.2020.1799865.

[36] Aouad, M. R.; Khan, D. J. O.; Said, M. A., *et al*., Novel 1,2,3-Triazole Derivatives as Potential Inhibitors against Covid-19 Main Protease: Synthesis, Characterization, Molecular Docking and DFT Studies. *Chem. Select* **2021**, *6* (14), 3468-3486, DOI: 10.1002/slct.202100522.

[37] Chikhale, R. V.; Sinha, S. K.; Patil, R. B.; Prasad, S. K.; Shakya, A.; Gurav, N.; Prasad, R.; Dhaswadikar, S. R.; Wanjari, M.; Gurav, S. S., *In-silico* Investigation of Phytochemicals from Asparagus Racemosus as Plausible Antiviral Agent In COVID-19. *J. Biomol. Struct. Dyn.* **2021**, *39* (14), 5033-5047, DOI: 10.1080/07391102.2020.1798813.

[38] Pant, S.; Singh, M.; Ravichandiran, V.; Murty, U. S. N.; Srivastava, H. K., Peptide-like And Small-molecule Inhibitors Against Covid-19. *J. Biomol. Struct. Dyn.* **2020**, *39* (8), 2904-2913, DOI: 10.1080/07391102.2020.1757510.

[39] Vijayan, V.; Pant, P.; Vikram, N., *et al*., Identification of Promising Drug Candidates Against NSP16 of SARS-CoV-2 Through Computational Drug Repurposing Study. *J. Biomol. Struct. Dyn.* **2021**, *39* (17), 6713-6727, DOI: 10.1080/07391102.2020.1802349.

[40] Vijayakumar, B.; Karthik, L., Screening of FDA Approved Drugs Against SARS-CoV-2 Main Protease: Coronavirus Disease. *Int. J. Pept. Res. Ther.* **2021**, *27* (1), 651-658, DOI: 10.1007/s10989-020-10115-6.

[41] Abdellatiif, M. H.; Ali, A.; Ali, A.; Hussien, M. A., Computational Studies by Molecular Docking of Some Antiviral Drugs with COVID-19 Receptors Are An Approach to Medication for COVID-19. *Open Chem.* **2021**, *19* (1), 245-264, DOI: 10.1515/chem-2021-0024.

[42] Pintilie, L.; Tanase, C.; Mohapatra, R. K., Molecular Docking Studies on Synthetic Therapeutic Agents for COVID-19. *Chem. Proc.* **2021**, *3* (1), 46, DOI: 10.3390/ecsoc-24-08352.

[43] Pitsillou, E.; Liang, J., Ververis, K., Lim, K. W., Hung, A., Karagiannis, T. C., Identification of Small Molecule Inhibitors of The Deubiquitinating Activity of The SARS-CoV-2 Papain-like Protease: In Silico Molecular Docking Studies And *In Vitro* Enzymatic Activity Assay. *Front. Chem.* **2020**, *8*, 623971, DOI: 10.3389/fchem.2020.623971.

[44] Kalhotra, P.; Chittepu, V. C. S. R.; Osorio-Revilla, G.; Gallardo-Velazquez, T., Field-template, QSAR, Ensemble Molecular Docking, And 3D-RISM Solvation Studies Expose Potential of FDA-approved Marine Drugs as SARS-CoVID-2 Main Protease Inhibitors. *Molecules* **2021**, *26* (4), 936-947, DOI: 10.3390/molecules26040936.

[45] Al-Douh, M. H.; Selim, E. A. B.; Abdallah, H. H.; Abdullah, H. Y.; Al-Bakri, A. K.; Al–Nohey, D. S.; Mahram, S. M. B.; Yusr, K. M.; Hawiel, F. A. B., Molecular Docking Study of Some Nitro Diazo Dye Derivatives as Antiviral Candidates of COVID-19. *Asian J. Appl. Chem. Res.* **2021**, *8*, 8-15, DOI: 10.9734/ajacr/2021/v8i230187.

[46] Guler, H. I.; Tatar, G.; Yildiz, O.; Belduz, A. O.; Kolayli, S., Investigation of Potential Inhibitor Properties of Ethanolic Propolis Extracts Against ACE-II Receptors for COVID-19 Treatment by Molecular Docking Study. *Arch. Microbiol.* **2021**, *203* (6), 3557-3564, DOI: 10.1007/s00203-021-02351-1.

[47] Sabet, R.; Sisakht, M.; Emami, L.; Sabahi, Z., Comparison of COVID-19 Virus Main Protease Inhibition Activities of Phenolic Acids by Molecular Docking. *Trends Pharmacol. Sci.* **2021**, *7* (2), 117-126, DOI: 10.30476/tips.2021.90386.1083.

[48] Morgon, N. H.; Grandini, G. S.; Yoguim, M. I., *et al*., Potential Activity of Linezolid Against SARS-CoV-2 Using Electronic And Molecular Docking Study. *J. Mol. Model.* **2021**, *27* (8), 222, DOI: 10.1007/s00894-021-04828-8.

[49] Nielsen, A. B.; Holder, A. J., GaussView 5.0. **2009**, User's Reference. GAUSSIAN Inc., Pittsburgh.

[50] Rappe, A. K.; Casewit, C. J.; Colwell, K. S.; Goddard III, W. A.; Skiff, W. M., UFF, A Full Periodic Table Force Field for Molecular Mechanics And Molecular Dynamics Simulations. *J. Amer. Chem. Soc.* **1992**, *114* (25), 10024-10035, DOI: 10.1021/ja00051a040.

[51] Frisch, M. J.; *et al*., *Gaussian 03*(Gaussian, Inc., Wallingford, CT, **2003**)

[52] Protein Data Bank (https://www.rcsb.org/)

[53] Morris, G. M.; Huey, R.; Lindstrom, W.; Sanner, M. F.; Belew, R. K.; Goodsell, D. S.; Olson, A. J., AutoDock4 And AutoDockTools4: Automated Docking with Selective Receptor Flexibility. *J. Comput. Chem.* **2009**, *30* (16), 2785-2791, DOI: 10.1002/jcc.21256.

[54] Trott, O.; Olson, A. J., AutoDock Vina: Improving The Speed and Accuracy of Docking with ANew Scoring Function, Efficient Optimization, and Multithreading. *J. Comput. Chem.* **2010**, *31* (2), 455-461, DOI: 10.1002/jcc.21334.

[55] Openbable (http://openbabel.org/wiki/Main_Page)

[56] Yin, W.; Mao, C.; Luan, X.; Shen, D. D.; Shen, Q.; Su, H.; Wang, X.; Zhou, F.; Zhao, W.; Gao, M.; Chang, S., Structural Basis for Inhibition of The RNA-dependent RNA Polymerase from SARS-CoV-2 by Remdesivir. *Science* **2020**, *368* (6498), 1499-1504, DOI: 10.1126/science.abc1560.

[57] Hoffmann, M.; Kleine-Weber, H.; Schroeder, S., *et al*., SARS-CoV-2 cell entry depends on ACE2 and TMPRSS2 and as blocked by a clinically proven protease inhibitor. *Cell* **2020**, *181*, 271-280, DOI: 10.1016/j.cell.2020.02.052.

[58] Jain, A. N., Scoring Functions for Protein-Ligand Docking. *Curr. Protein Pept. Sci.* **2006***, 7* (5), 407-420, DOI: 10.2174/138920306778559395.

[59] Jorgensen, S. C. J.; Kebriaei, R.; Dresser, L. D., Remdesivir: Review of Pharmacology, Pre-clinical Data, And Emerging Clinical Experience for COVID-19. *Pharmacotherapy* **2020**, *40* (7), 659-671, DOI: 10.1002/phar.2429.

[60] Sanders, J. M.; Monogue, M. L., Jodlowski, T. Z., Cutrell, J. B., Pharmacologic Treatments for Coronavirus Disease 2019 (COVID-19): A Review. *J. Amer. Med. Assoc*. **2020**, *323* (18), 1824-1836, DOI: 10.1001/jama.2020.6019.

[61] Holman, W.; Holman, W.; McIntosh, S., et al.,Accelerated First-in-human Clinical Trial of EIDD-2801/MK-4482 (Molnupiravir), A Ribonucleoside Analog With Potent Antiviral Activity Against SARS-CoV-2. *Trials*. **2021**, *22* (1), 561, DOI: 10.1186/ s13063-021-05538-5.

[62] BIOVIA Discovery Studio **2021**: Friday, October 23, **2020**; https://discover.3ds.com/discovery-studio-visualizer-download.

[63] Pettersen, E. F.; Goddard, T. D.; Huang, C. C.; Couch, G. S.; Greenblatt, D. M.; Meng, E. C.; Ferrin, T. E., UCSF Chimera? A Visualization System for Exploratory Research And Analysis. *J. Comput. Chem.* **2004**, *2 5* (13), 1605-1612,DOI: 10.1002/jcc.20084. https://www.cgl.ucsf.edu/chimera/docs/relnotes.html.

[64] Tavakol, S.; Seifalian, A. M.,Vitamin E at A High Dose as An Anti-ferroptosis Drug And Not Just A Supplement for COVID-19 Treatment. *Biotechnol. Appl. Biochem.* **2021**, PMID: 33938041, DOI: 1010.1002/bab.2176.

[65] Darbar, S.; Saha, S.; Agarwal, S., Immunomodulatory Role of Vitamin C, D and E to Fight Against COVID-19 Infection Through Boosting Immunity: A Review. *Parana J. Sci. Educ.* **2021**, *7* (1), 10-18. http://tiny.cc/PJSE24476153v7i1p010-018.